En masse in vitro functional profiling of the axonal mechanosensitivity of sensory neurons

Dmitry Usoskin[a], Misha Zilberter[a], Sten Linnarsson[a], Jens Hjerling-Leffler[a,b], Per Uhlén[a], Tibor Harkany[a,c], and Patrik Ernfors[a,1]

[a]Department of Medical Biochemistry and Biophysics, Karolinska Institutet, S-17177 Stockholm, Sweden; [b]Smilow Neuroscience Program, New York University School of Medicine, New York, NY 10016; and [c]European Neuroscience Institute at Aberdeen, University of Aberdeen, Aberdeen AB25 2ZD, United Kingdom

Edited* by Tomas G. M. Hökfelt, Karolinska Institutet, Stockholm, Sweden, and approved July 19, 2010 (received for review December 18, 2009)

Perception of the environment relies on somatosensory neurons. Mechanosensory, proprioceptor and many nociceptor subtypes of these neurons have specific mechanosensitivity profiles to adequately differentiate stimulus patterns. Nevertheless, the cellular basis of differential mechanosensation remains largely elusive. Successful transduction of sensory information relies on the recruitment of sensory neurons and mechanosensation occurring at their peripheral axonal endings in vivo. Conspicuously, existing in vitro models aimed to decipher molecular mechanisms of mechanosensation test single sensory neuron somata at any one time. Here, we introduce a compartmental in vitro chamber design to deliver precisely controlled mechanical stimulation of sensory axons with synchronous real-time imaging of Ca^{2+} transients in neuronal somata that reliably reflect action potential firing patterns. We report of three previously not characterized types of mechanosensitive neuron subpopulations with distinct intrinsic axonal properties tuned specifically to static indentation or vibration stimuli, showing that different classes of sensory neurons are tuned to specific types of mechanical stimuli. Primary receptor currents of vibration neurons display rapidly adapting conductance reliably detected for every single stimulus during vibration and are consistently converted into action potentials. This result allows for the characterization of two critical steps of mechanosensation in vivo: primary signal detection and signal conversion into specific action potential firing patterns in axons.

compartmentalized chamber | dorsal root ganglion | neurite | end-organ | vibration

Continuous sensing of the surrounding environment is an absolute requirement for any organism to ensure its survival through adaptation. Recently, significant progress has been made in understanding the molecular mechanisms underpinning the perception of temperature and chemical stimuli in both vertebrates and invertebrates (1–3). In contrast, the molecular and cellular requirements for mechanoreception during sensations of touch and pain have yet to be elucidated.

The application of mechanical force is believed to activate ion channels in sensory nerve endings, resulting in membrane depolarization and peripheral action potential (AP) generation (4, 5). Nociceptors contain free nerve endings acting as high-threshold mechanotransducers. Vibration, touch, and pressure sensations are mediated by low-threshold myelinated sensory afferents with their unmyelinated terminals located within specialized accessory structures, the sensory end-organs (6). Our ability to discriminate fine modalities of mechanical stimuli is thought to be underlain by multiple subtypes of myelinated sensory neurons, each associated with corresponding sensory end-organs. However, the relative importance of sensory end-organs vs. intrinsic mechanoreceptive properties of neurons themselves remains elusive, largely because of the lack of models to resolve neuronal responses to diverse stimuli in the absence of end-organs.

Sensory neurons' mechanoreception is conventionally assessed in soma-free ex vivo skin-nerve preparations (7, 8) or in dissociated neurons using direct somatic stimulation to mimic mechanoreception in the absence of an end-organ (9–14). Neither approach allows for analyzing the full complexity of mechanosensation—from different types of stimuli—receptor current (RC)-evoked depolarization to the stimuli's final translation into a specific AP pattern.

To decipher the functional complexity of mechanosensory neuron subtypes, we have designed an in vitro compartmentalized chamber system to evaluate how axons discriminate among diverse sensory inputs and encode particular stimuli into specific AP patterns. This system is achieved by applying a precise stimulus pattern onto axons grown inside a cushion gel, a semipermeable target of innervation, while synchronously monitoring somatic responses by means of real-time Ca^{2+} imaging (15, 16) and electrophysiology. We demonstrate that Ca^{2+} imaging is a predictor of electrical activity and that the soma represents an accurate "attached" sensor of electrical activity triggered by the primary stimulus applied to the neurites. Thus, we can conclusively identify functionally distinct mechanosensory neuron subpopulations based on their unique pharmacological, electrophysiological, and neurochemical properties.

Results

Compartmentalized Cell-Based System with Controlled Mechanical Stimulation to Neurites. We designed a compartmentalized chamber with a cushion gel allowing delivery of precise mechanical stimuli (*SI Materials and Methods* and Fig. S1*A*). After a period of 4 to 6 d following seeding dissociated sensory neurons from mouse dorsal root ganglia into the central compartment, the cells extended their axons into the gel block in a gradient of a mixture of growth factors (NGF, BDNF, NT3, and glial cell line-derived neurotrophic factor). The block itself is covered by a piece of flexible plastic (below referred to as a "bridge") and represents an adjacent compartment (Fig. S1 *B–D‴*). Mechanical stimuli were delivered to axon endings by vertical displacement of the bridge via a computer-controlled piezo probe (Fig. S1 *E* and *F*). Axonal stimulation resulted in somatic responses in the majority of cells as reported by Ca^{2+} imaging (Fig. 1). This stimulation was followed by sequential perfusion of the central chamber with capsaicin and KCl to reveal nociceptors and to detect all electrically active neurons (Fig. 1 *A–C*), respectively.

Static and Vibration-Sensitive Neurons. When applying a train of consecutive indentation stimuli (i.e., static stimulation) of increasing magnitude, we find that $94 \pm 4\%$ of neurons that responded

Author contributions: D.U. and P.E. designed research; D.U., S.L., J.H.-L., P.U., and T.H. performed research; M.Z. performed electrophysiological recording; D.U. and M.Z. analyzed data; and D.U., M.Z., T.H., and P.E. wrote the paper.

The authors declare no conflict of interest.

*This Direct Submission article had a prearranged editor.

Freely available online through the PNAS open access option.

[1]To whom correspondence should be addressed. E-mail: patrik.ernfors@ki.se.

This article contains supporting information online at www.pnas.org/lookup/suppl/doi:10.1073/pnas.0914705107/-/DCSupplemental.

www.pnas.org/cgi/doi/10.1073/pnas.0914705107

Downloaded at Palestinian Territory, occupied on December 17, 2021

www.manaraa.com

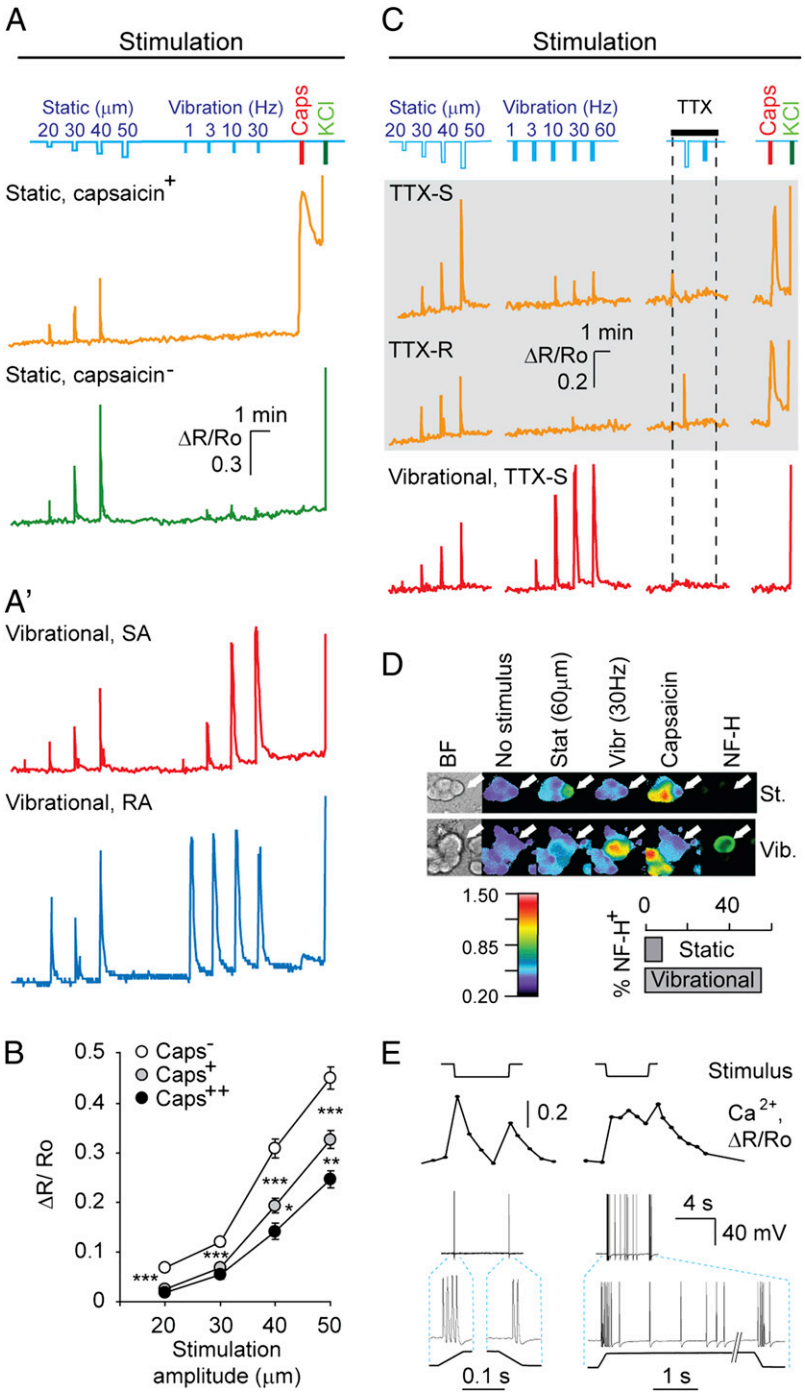

Fig. 1. Classification of sensory neuron subtypes by their response characteristics. (*A* and *A'*) Single Ca^{2+} traces of cells representing different functional populations identified in culture. Mechanical stimulation profiles are depicted on the top in blue. Each stimulation train was followed by somatic stimulation with capsaicin and KCl. (*B*) Ca^{2+} responsiveness to mechanical stimulation negatively correlates with responsiveness to capsaicin. Cells were grouped into categories based on Ca^{2+} level change in response to capsaicin (Caps) stimulations: 40% weakest responders ($Caps^{-}$, $n = 141$, $N = 3$), 40% midresponders ($Caps^{+}$, $n = 134$, $N = 3$), and 20% strong responders ($Caps^{++}$, $n = 50$, $N = 3$). Mean amplitude for Ca^{2+} response was calculated in each group for stimulations of each magnitude for those cells, which (*i*) exceeded a threshold of 0.2 for at least one static stimulation, and (*ii*) did not exceeded a threshold of 0.4 for any vibration stimuli. $*P = 0.075$; $**P = 0.044$; $***P < 0.001$ (Mann-Whitney test). (*C*) Representative traces of TTX-R and TTX-S cells. Static (gray background) and vibration stimuli were applied as indicated in the presence of 1 μM TTX in the central chamber. (*D*) (*Upper*) Bright field and pseudocolored ratiometric Ca^{2+} imaging responses and NF-H immunoreactivity of representative cells of static and vibrational populations. (*Lower*) Percentage of $NF\text{-}H^{+}$ cells among static and vibration populations. (*E*) Representative Ca^{2+} responses triggered by static stimulation, coupled with simultaneous electrophysiological recording from neuronal soma. Prototypic slowly adapting (SA) and rapidly adapting (RA) responses were identified. Note that the Ca^{2+} level change reflects the pattern of APs.

to a low-intensity stimulus were also responsive to higher-stimulus magnitudes as determined by the amplitude of somatic Ca^{2+} transient (threshold = 0.2; $n = 284$ neurons, $N = 3$ experiments). The distance from soma to the bridge had no effect on the neurons' response profiles or sensitivity (*SI Materials and Methods* and Fig. S2*A*). Graded responses were detected in 79 ± 7% of neurons

NEUROSCIENCE
Downloaded at Palestinian Territory, occupied on December 17, 2021
www.manaraa.com

(n = 284, N = 3) (Fig. 1*A*). A 79 ± 3% of neurons responsive to mechanical stimulation were activated by static indentation and not by a sinusoidal vibration stimulus (5 s) with the frequency varying between 1 and 60 Hz. We classify these as "static" neurons.

Two identical consecutive static stimuli resulted in similar Ca^{2+} responses, demonstrating the reliability of our recording method (Fig. S2*B*). A portion of static responsive neurons responded to capsaicin (38 ± 2%; n = 284, N = 3) (Fig. 1*A*). Responsiveness to mechanical stimulation was found to inversely relate to capsaicin sensitivity: the higher the static neuron's sensitivity was to capsaicin, the lower it was to mechanical stimulation (Fig. 1*B*). This finding suggests that cells with capsaicin sensitivity, a hallmark feature of nociceptors, demonstrate a high threshold for mechanical stimulus response, which is in agreement with a previous in vitro study (9).

Trains of vibration stimuli were applied to identify neurons specifically tuned to this type of stimulus in vivo (17, 18): 21 ± 3% of mechanosensitive neurons reliably responded to vibration stimuli (henceforth termed "vibration neurons") (Fig. 1*A′*). Vibration neurons did not respond to capsaicin stimulation (n = 1/152, N = 6) (Fig. 1 *A′* and *C*) and, unlike static neurons, were neurofilament heavy chain (NF-H)-positive (Fig. 1*D*), indicating that nociceptors belong to the subpopulation of static neurons, because nociceptive neurons are of small diameter, unmyelinated, and lack NF-H immunoreactivity in vivo (19).

To confirm that Ca^{2+} transients observed in the soma are mediated by APs generated at the site of stimulation, we applied tetrodotoxin (TTX), a voltage-gated sodium channel blocker, which acts predominantly on nonnociceptive sensory neurons (20, 21). Application of TTX (1 μM) to the central chamber abolished the response of all of the vibration neurons [classified as TTX-sensitive (TTX-S); n = 34, N = 2] (Fig. 1*C*). We find that 47% of static neurons (both capsaicin-sensitive and insensitive) were TTX-resistant (TTX-R) (n = 111, N = 2) (Fig. 1*C*), further emphasizing that nociceptors belong to the static neuron subpopulation.

To reveal the specific patterns of APs triggered by the mechanical stimulation at the axonal level, whole-cell recordings with simultaneous Ca^{2+} imaging were performed during application of different stimuli. Static stimulation evoked two firing profiles, one exhibiting a typical rapidly adapting response, with only brief trains of APs at the onset and often at the end of stimulation (n = 25 cells) (Fig. 1*E*). Three out of 28 cells also displayed additional firing during the tonic phase of stimulation (Fig. 1*E*).

Subclasses of Vibration-Responsive Neurons. Vibration neurons represent 21% of all observed mechanoresponsive neurons ($n_{vibration}$ = 158, N = 8) (Fig. 1*A′*). These neurons form two subtypes that differ in their response profile to a series of vibrations with incrementing frequency, and are therefore referred to as slowly adapting or rapidly adapting vibration neurons (V-SA and V-RA, respectively) (Figs. 1*A′* and 2 *A* and *B*). V-SA neurons exhibited a stronger response to higher stimulus frequencies (Fig. 2*A* and *B*). In contrast, V-RA neurons responded to low frequency range (3 and 10 Hz), similarly to V-SA neurons, but showed comparatively lower response amplitudes at higher frequencies (30 and 60 Hz).

Series of vibration stimuli (10 Hz) of increased duration (4, 8, and 12 s) revealed that V-SA but not V-RA cells displayed persistently high levels of intracellular Ca^{2+} throughout the duration of the stimulus (Fig. 3*A*) ($P < 0.001, n = 38, N = 4$). Both V-SA and V-RA neurons also demonstrated reproducible responses to two identical vibration stimuli (Fig. S2*C*). V-SA neurons had larger somatic diameter than V-RA neurons (Fig. 3 *B* and *B′*), but V-RA and static neurons did not differ in their soma sizes. V-RA neurons responded stronger to static stimuli than V-SA neurons (Fig. 2*C*).

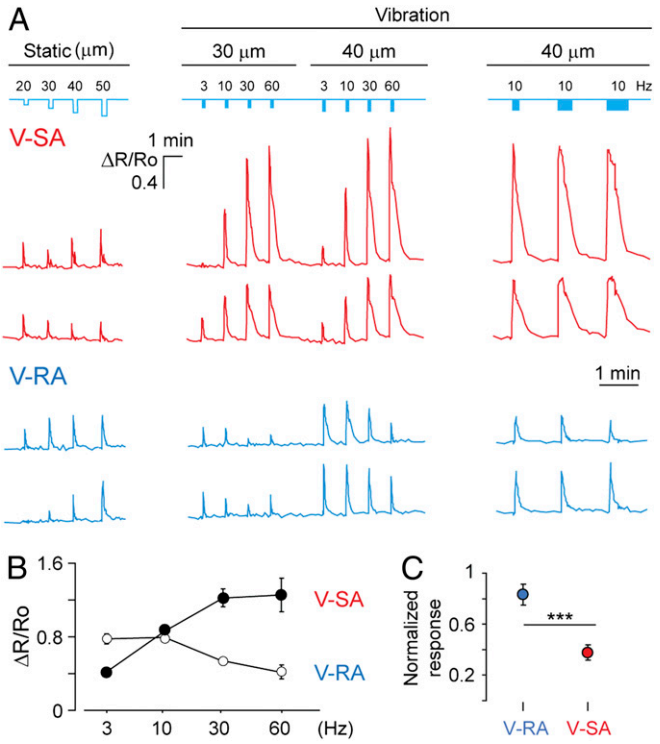

Fig. 2. Subclass specificity of vibration-sensitive neurons. (*A*) Representative Ca^{2+} traces of cells from two vibrational cell subpopulations. Mechanical stimulation profile is depicted on the top in blue. Note that the last three vibration stimulations are of increasing duration, as indicated by bar thickness (4, 8, and 12 s). (*B*) Response profile of V-SA (n = 29; N = 2) and V-RA (n = 30; N = 2) neurons to vibrational stimulation of different frequency plotted as a mean of Ca^{2+} transients' amplitude. (*C*) V-RA and V-SA neuron responsiveness to static stimulation normalized to vibrational response. ***$P <$ 0.001 (Mann-Whitney test).

Discharge Properties of V-SA and V-RA Neurons. Whole-cell recording with synchronous Ca^{2+} imaging revealed a characteristic discharge pattern that accounts for the difference between observed Ca^{2+} response profiles of V-SA and V-RA neurons. Typically, neurons with V-SA-like Ca^{2+} response profiles were active throughout the duration of a vibration stimulus (with the exception of 3-Hz stimulation, where an adaptation of AP frequency was sometimes observed) (Fig. 4*A*). Unlike V-SA neurons, V-RA cells exhibited rapid adaptation during the course of stimulation (Fig. 4*A*). In addition, similar firing patterns consisting of several APs evoked by 3-Hz stimulation appeared to result in Ca^{2+} transients, which were larger in V-RA than those in V-SA neurons (Fig. 4*A*). V-RA neurons displayed faster adaptation at higher vibration frequencies, which could account for their lower Ca^{2+} response seen at 30- or 60-Hz vibration stimulation (Fig. 4*A*). APs and corresponding Ca^{2+} transients recorded during 10-Hz vibration stimulation of different durations (4, 8, and 12 s) revealed the same tendency: V-SA neurons generated a continuous discharge of APs with little adaptation and exhibited a high and steady level of Ca^{2+} throughout the full duration of the stimulation (Fig. 3*A*). In contrast, V-RA neurons ceased firing shortly after the onset of stimulus, resulting in a rapidly decaying Ca^{2+} transient (Fig. 3*A*).

The difference in AP discharge properties between V-SA and V-RA neurons was also reflected in the delay from the stimulus onset to the peak of Ca^{2+} transient. Although the delay to $[Ca^{2+}]$ peak for a 3-Hz stimulation was similar in both neuronal types, at higher frequencies this parameter became reduced in V-RA, but not in V-SA neurons (Fig. 4*B*). This result is likely because of a faster AP firing frequency adaptation exhibited by V-RA neurons.

Downloaded at Palestinian Territory, occupied on December 17, 2021
www.manaraa.com

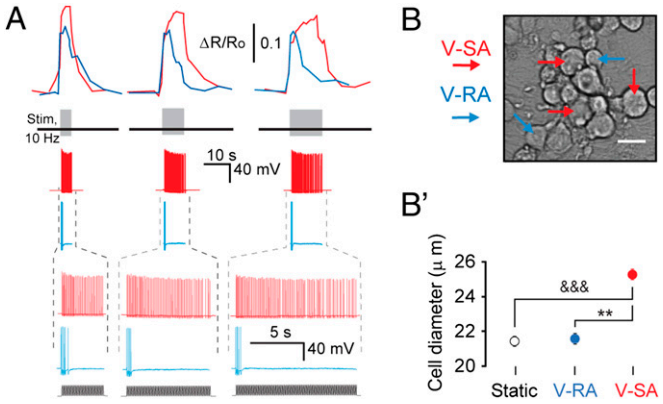

Fig. 3. Cellular responses to vibration stimuli. (*A*) From the top in each column: Ca^{2+} transients; position of vibration stimuli on the time axis; membrane potential recording (whole-cell mode); time zoom of above potential recording with the profile of vibration stimuli presented underneath. Application of 10-Hz vibration of different duration (4, 8, and 12 s) confirmed that V-SA adapt to this type of stimulus to a much lesser extent than V-RA neurons. The differential responsiveness of V-SA and V-RA neurons correlates with their [Ca^{2+}] transients over the entire period of stimulation. (*B* and *B'*) V-SA neurons have larger somatic diameter than V-RA neurons. Brightfield view (*B*) of V-SA (red arrows) and V-RA (blue arrows) somata, and their quantitative comparison (*B'*). $^{\&\&\&}P < 0.001$; $^{**}P < 0.01$ (Mann-Whitney test).

RC Recordings. Previous paradigms allowed for recording of either the AP firing profile from mechanically stimulated axons in skin-nerve preparation (7, 8), or somatic/proximal axon RCs in dissociated neuronal culture (9, 21). Questionably, these two phenomena were suggested to be related even though data were obtained under different experimental paradigms. Here, we set out to record the RCs of V-SA neurons and their correlation to AP firing patterns, following both static and vibration stimuli. For this purpose, a Capron fiber was positioned above the axons within the gel to provide highly focal stimuli (Fig. S3). V-SA neurons were first identified based on Ca^{2+} transients and their AP patterns were recorded, followed by application of TTX (1 μM) to block APs and isolate the RCs. Following weak static stimulus (25-μm indendation, 1 s) a single AP was recorded at the onset of the stimulus. The corresponding RC underlying the AP was a fast inward current measured in voltage-clamped (−60 mV) cell soma (Fig. 5*A*). The currents had a mean peak amplitude of 70 pA. The latency between onset of stimuli and current activation was rapid (6.5 ms at an indentation ramp of 3 mm/s) (Fig. 5*A*). The latency to response was dependent on the ramp of stimulus with a delayed current activation at a slower ramp (17 ms at a ramp of 0.9 mm/s) (Fig. 5*A*). Fitting the RC traces with single exponential functions to calculate the time constant for current inactivation produced tau values of 22.2 ± 0.7 ms and 17.1 ± 0.2 ms for RCs recorded at ramps of 0.9 mm/s and 3 mm/s, respectively. The ramp-dependent kinetics indicate that the mechanical stimulus directly gates ion channels.

In agreement with our previous findings, vibration stimuli (30 Hz, 1 s) led to continuous discharge of APs without significant fatigue, although not all cycles successfully initiated an AP (Fig. 5*A*). In contrast, RCs were reliably detected for every single stimulus during the vibration. Thus, in V-SA neurons, the RC is reliably converted to an AP during the vibration stimulus. The mean peak amplitude of the current declined with each successive cycle during the vibration before reaching steady-state levels (2.3 ratio of first three RCs to the last three RCs during a 1-s stimulus).

Prevalence of Different Subcategories of Mechanosensitive Neurons. Based on the mechanosensitive properties revealed by our method, neurons were classified into further subcategories of cells responding to static indentation, vibration, and capsaicin, as well as those either sensitive or resistant to TTX (Fig. 5*B*). Static neurons were by far the most prevalent type, making up 79% of the entire population. Of these neurons, 38% also responded to capsaicin. TTX resistance was observed exclusively among the static neurons and was present in 47% of them, independent of capsaicin sensitivity. Vibration neurons made up 21% of all mechanical stimulus-responding cells: V-SA contributed with 8 ± 2%, and V-RA provided the remaining 13 ± 3%. All vibration neurons were NF-H^+, TTX-sensitive and did not respond to capsaicin (vibration neurons $n = 152$, $N = 6$).

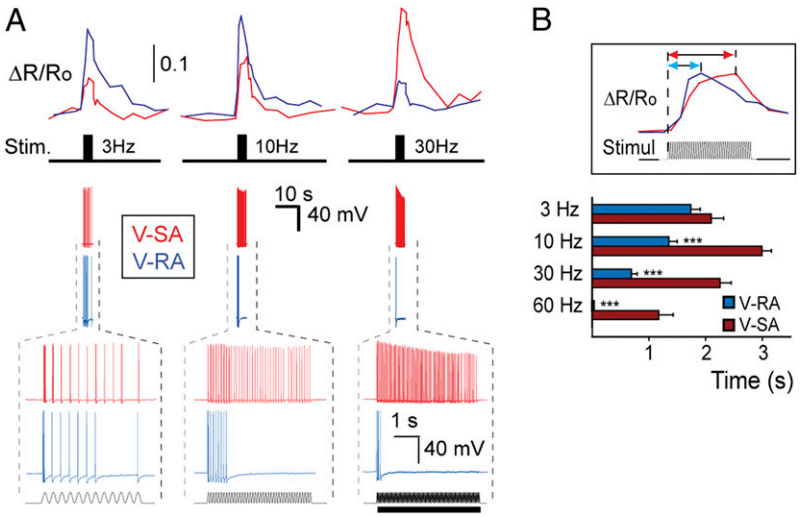

Fig. 4. Correlated Ca^{2+} dynamics and discharge patterns of vibration-sensitive neurons. (*A*) Ca^{2+} imaging with simultaneous electrophysiological recording reveals the difference between V-SA (red traces) and V-RA (blue traces) cells in both adaptation properties and Ca^{2+} dynamics. From the top in each column: Ca^{2+} transients; position of vibration stimuli on the time axis; membrane potential recording (whole-cell); time zoom of above potential recording. (*Bottom trace*) Profile of vibrational stimulation. (*B*) Delay between the vibration stimulus onset and Ca^{2+} transient maximum for high frequencies is smaller for V-RA ($n = 30$; $N = 2$) than for V-SA neurons ($n = 29$; $N = 2$). Asterisks depict significance between delay for V-RA and V-SA neurons for the same frequency of stimulation. $^{***}P < 0.001$ (Mann-Whitney test).

Downloaded at Palestinian Territory, occupied on December 17, 2021
www.manaraa.com

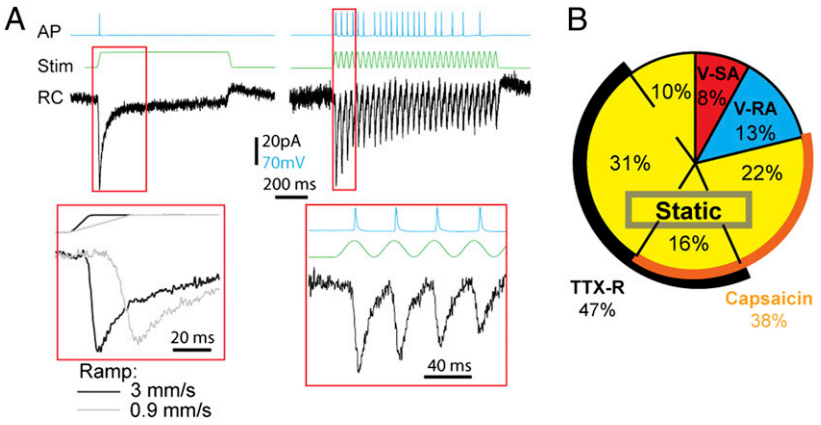

Fig. 5. RC recordings in vitro. (*A*) Sensory neurons generate RCs during both static (*Left*) and vibration (*Right*) stimulation in the presence of TTX. AP firing profile and corresponding RCs during static stimulation of different ramping speeds (*Lower Left*) and 30-Hz vibrational stimulus (*Lower Right*). (*B*) Proportion of main mechanosensitive sensory neuron populations as identified with the techniques introduced in this article. Pie chart with percentages of sensory neurons responding to the stimuli indicated, and the sensitivity of their subpopulations to TTX or capsaicin.

Discussion

Cell-culture systems allowing for placement of cell somata and neurites in separate compartments were introduced more than a decade ago (22). Although these systems were extensively used for biochemical studies, several technical limitations prevented them from being used for assessing axonal mechanosensitivity, one of the key unresolved issues in sensory biology today. Our paradigm overcomes these complications yet preserves the advantages of compartmentalization by introducing a gel-cushion compartment. Our model offers the possibility to record from dozens to hundreds of cells simultaneously, with precisely controlled mechanical stimulation applied selectively to sensory axons. The first aspect efficiently deals with the problem of sensory neuron heterogeneity, avoiding the need for extensive testing of cells one by one. Additionally, using the cell soma as a model for axonal mechanosensitivity may not be fully adequate not only because of the ultrastructural differences of signal propagation between the structures, but also because such a model does not resolve the balance between RC and membrane excitability that establishes a response threshold [as it was recently reported for cold sensation (2)]. Our paradigm possesses the robustness of optical methods (several hundred cells per single experiment), but also allows for consequent recording of both the underlying receptor currents and the generated firing patterns, providing an ability to look for functional clues in cell preselection. Despite the low Ca^{2+} imaging rate (sampling at 1 Hz), the imaging method is sensitive enough to estimate the few APs occurring at the soma in a short burst (Fig. S4), but does not capture the kinetics of the receptor currents, which are much faster. The use of gel cushion in the distal compartment naturally opens a possibility to create specific microenvironments around the axonal endings, and thus to mimic the in vivo situation for addressing the role of end-organs in mechanoreception. In addition to studies of mechanosensitivity, our system can be adapted for selective application of thermal or chemical stimuli specifically to nerve terminals.

Our experimental paradigm revealed three types of mechanically sensitive neurons, those responding exclusively to static indentation as well as two types of vibration-responsive neurons. Cells responsive to capsaicin and resistant to TTX (i.e., prototypic nociceptors) were found to be exclusively among the static neuron group. Interstingly, one in vivo study (23) reported that TRPV1-expressing nociceptors are mechanically insensitive in vivo, indicating that a subpopulation of cells in our system develop capsaicin sensitivity during culturing. Reported down-regulation of the TTX-R sodium channels $Na_v1.8$ and $Na_v1.9$ after peripheral nerve axotomy (24) could explain the fact that not all capsaicin-responsive cells were TTX-resistant. Depending on their sensitivity to the stimulus, skin mechanoreceptors can be classified as low or high threshold, the latter being mechanonociceptors (4, 6). In our study, we could not separate the two mechanoreceptor populations based solely on the threshold of their activation. However, responsiveness to capsaicin marks presumable nociceptors, which in our paradigm are also weak responders to mechanical stimuli. The failure to distinguish between the low- and high-threshold mechanoreceptor types in our system could indicate an important role of the end-organ structure (presently absent in our system), which could serve to lower the sensitivity level for low-threshold mechanosensors. Consistent with this suggestion, a recent study reports that mice lacking Merkel cells demonstrate a complete loss of neurophysiological responses mediated by the Merkel cell-neurite complex (25).

We also identified two distinct types of vibration-responsive neurons. The V-SA neurons were slowly adapting to vibration, had a larger somatic diameter, showed a weaker response to static indentation (Figs. 3 *B* and *B′* and 2*C*), and demonstrated continuous AP discharge throughout the stimulus duration. The V-RA neurons rapidly adapted to vibration stimulation, had a smaller cell soma, and displayed a stronger Ca^{2+} response to static indentation. The latter difference between the two vibration neuron types could be explained by differing somatic Ca^{2+} dynamics in response to APs, as suggested by the observation that similar numbers of APs triggered a stronger Ca^{2+} response in V-RA than in V-SA neurons (Fig. 4*A*, 3-Hz stimulation). Hence, we have identified qualitatively different, cell-specific intrinsic properties of vibration stimulus responses. The most prominent populations of neurons sensitive to vibration are Pacinian corpuscles, Meissner corpuscles, and lanceolate endings associated with hair follicles, all of which are of the rapidly adapting type of neurons. Intriguingly, the nonneural accessory structure surrounding the central unmyelinated axon of Pacinian corpuscles determines its adaptation, and removal of this connective tissue transforms the neuron from a RA to a SA receptor in terms of the generator potential (26). Nevertheless, the direct relationship between the V-SA and V-RA neurons and the neural components of Pacinian and Meissner corpuscles remains to be determined.

In addition to determining the response characteristics of mechanosensitive neurons, our model offers a potential to study the underlying mechanisms of response differentiation as well as of mechanosensation itself. Recording of RCs from stimulated axons together with the corresponding AP firing pattern allowed for the elucidation of both the response characteristics of me-

Downloaded at Palestinian Territory, occupied on December 17, 2021
www.manaraa.com

chanical gating in axons and the mechanisms of its translation into the AP firing profile. The RC was similar to RA currents previously reported in mechanosensitive neurons (21), and revealed a reliable current for each sinusoidal vibration stimulus that was consistently converted into APs in V-SA neurons, with only a very small reduction in current peak amplitude following long trains of stimuli.

Despite an intense effort of elucidating the cellular and molecular basis of mechanosensitivity, much remains unknown (11, 27–32). We believe that our unique experimental technique allows for detailed studies of cell-autonomous mechanisms and should facilitate future efforts at resolving the molecular basis of mechanotransduction. Our method might also be suitable for addressing the role of different cellular components, such as the nonneural Merkel cells (6, 33).

Materials and Methods

Mechanical Stimulation. A piezo bender with an attached iron pin (probe) was used to provide mechanical stimulation by positioning the pin in contact with the top of the gel bridge (Fig. S1*A*). The thickness of the MG "sandwich" under the gel bridge was ~270 μm. The magnitude of applied mechanical stimulation (indentation distance) varied from 20 to 80 μm (see *SI Materials and Methods* for details).

Ca^{2+} Imaging. Cell-loading with Fura-2/AM (Molecular Probes) and perfusion stimulation of somata were performed as described (34), with the exception of the final Fura-2/AM concentration being 4 μM. Ratiometric Ca^{2+} imaging was performed according to ref. 35, except that an 25× water immersion objective was used. $\Delta R/R_o = (R - R_o)/R_o$ was calculated to measure cellular responses, where R is the F340/F380 ratio and R_o is a baseline ratio before stimulus onset. Ca^{2+} imaging acquisition rate was 0.1 to 0.2 Hz between and 1 Hz during stimulations. The stimuli were applied at intervals of >1 min.

Electrophysiology. Target cells were identified by their response properties to mechanical stimulation using Ca^{2+} imaging. ΩOhm seals were obtained, followed by acquiring a whole-cell configuration in current clamp mode. To exclude any possible effect of artificial pipette solution on neuronal response properties, APs resulting from mechanical stimulation were recorded in cell-attached voltage-clamp mode (ΩOhm seals, noninvasive) by their corresponding capacitance current transients. Identical mechanical stimulation was then applied to the same cell and APs were recorded in whole-cell mode. No significant effect of pipette solution was observed. RCs were recorded in the presence of 1 μM TTX in the external solution and were averaged over a minimum of three sweeps. The pipette solution contained (in mM): 135 K-gluconate, 20 KCl, 4 ATP-Mg, 10 Na-phosphocreatine, 0.3 GTP, and 10 hepes, pH 7.3. Recordings were made using a Dagan PC-ONE amplifier (Dagan Corporation), sampled at 20 kHz, digitized by a Digidata interface (Axon Instruments/Molecular Devices), and analyzed off-line by P-Clamp software. Borosilicate glass patch pipettes had a resistance of 3 to 5 MΩ. Series resistance was not compensated.

Immunocytochemistry. After the experiment, cells were fixed with 4% paraformaldehyde in 0.1 M Na-phosphate buffer (pH 7.4) for 20 min on ice followed by immunocytochemical detection of select markers with monoclonal primary antibodies: anti-NF-H 200 (1:400; Sigma) and anti-β-III-tubulin (1:2,000; Promega). Species-specific secondary antibodies tagged with AlexaFluor 488 or carbocyanine 5 were used at a dilution range of 1:600 to 1:1,800.

Data Analysis. Preliminary visual analysis was performed using MetaFluor software (Molecular Devices). Throughout the text, *N* refers to the number of individual experiments and *n* the number of neurons recorded. Statistical analysis was performed in StatistiXL, an add-in for MS Excel. Two-tailed Mann-Whitney nonparametric test was used unless stated otherwise.

ACKNOWLEDGMENTS. This work was supported by the Swedish Research Council, Linné grants (Diploma in Biostatistics and Research Methodology grant), the Swedish Cancer Foundation and Swedish Child Cancer Foundation, the Swedish Brain Foundation, the Bertil Hållsten Research Foundation, the EU FP7 MOLPARK collaborative project, Karolinska Institutet strategic neuroscience program, Wallenberg Scholar and European Research Council Advanced Grant 232675 (to P.E.), the Wallenberg Foundation (CLICK facility at Molecular Neurobiology, Molecular Biology and Biochemistry, Karolinska Institutet) (P.U.), and The Swedish Society for Medical Research, Swedish Brain Foundation, and ELFA AB (D.U.). T.H. was supported by the EU FP7 MEMOLOAD project and the European Molecular Biology Organization Young Investigator Programme.

1. Bautista DM, et al. (2007) The menthol receptor TRPM8 is the principal detector of environmental cold. *Nature* 448:204–208.
2. Colburn RW, et al. (2007) Attenuated cold sensitivity in TRPM8 null mice. *Neuron* 54: 379–386.
3. Caterina MJ, et al. (1997) The capsaicin receptor: A heat-activated ion channel in the pain pathway. *Nature* 389:816–824.
4. Lewin GR, Moshourab R (2004) Mechanosensation and pain. *J Neurobiol* 61:30–44.
5. Gillespie PG, Walker RG (2001) Molecular basis of mechanosensory transduction. *Nature* 413:194–202.
6. Lumpkin EA, Caterina MJ (2007) Mechanisms of sensory transduction in the skin. *Nature* 445:858–865.
7. Koltzenburg M, Stucky CL, Lewin GR (1997) Receptive properties of mouse sensory neurons innervating hairy skin. *J Neurophysiol* 78:1841–1850.
8. Reeh PW (1986) Sensory receptors in mammalian skin in an in vitro preparation. *Neurosci Lett* 66:141–146.
9. Drew LJ, Wood JN, Cesare P (2002) Distinct mechanosensitive properties of capsaicin-sensitive and -insensitive sensory neurons. *J Neurosci* 22:RC228.
10. McCarter GC, Reichling DB, Levine JD (1999) Mechanical transduction by rat dorsal root ganglion neurons in vitro. *Neurosci Lett* 273:179–182.
11. Alessandri-Haber N, Dina OA, Chen X, Levine JD (2009) TRPC1 and TRPC6 channels cooperate with TRPV4 to mediate mechanical hyperalgesia and nociceptor sensitization. *J Neurosci* 29:6217–6228.
12. Cunningham JT, Wachtel RE, Abboud FM (1995) Mechanosensitive currents in putative aortic baroreceptor neurons in vitro. *J Neurophysiol* 73:2094–2098.
13. Bhattacharya MR, et al. (2008) Radial stretch reveals distinct populations of mechanosensitive mammalian somatosensory neurons. *Proc Natl Acad Sci USA* 105:20015–20020.
14. Zhang XF, Chen J, Faltynek CR, Moreland RB, Neelands TR (2008) Transient receptor potential A1 mediates an osmotically activated ion channel. *Eur J Neurosci* 27:605–611.
15. Clapham DE (2007) Calcium signaling. *Cell* 131:1047–1058.
16. Berridge MJ, Bootman MD, Roderick HL (2003) Calcium signalling: Dynamics, homeostasis and remodelling. *Nat Rev Mol Cell Biol* 4:517–529.
17. Talbot WH, Darian-Smith I, Kornhuber HH, Mountcastle VB (1968) The sense of flutter-vibration: Comparison of the human capacity with response patterns of mechanoreceptive afferents from the monkey hand. *J Neurophysiol* 31:301–334.
18. Koschorke GM, Meyer RA, Tillman DB, Campbell JN (1991) Ectopic excitability of injured nerves in monkey: entrained responses to vibratory stimuli. *J Neurophysiol* 65:693–701.
19. Woolf CJ, Ma Q (2007) Nociceptors—noxious stimulus detectors. *Neuron* 55:353–364.
20. García-Añoveros J, Samad TA, Zuvela-Jelaska L, Woolf CJ, Corey DP (2001) Transport and localization of the DEG/ENaC ion channel BNaC1alpha to peripheral mechanosensory terminals of dorsal root ganglia neurons. *J Neurosci* 21:2678–2686.
21. Hu J, Lewin GR (2006) Mechanosensitive currents in the neurites of cultured mouse sensory neurones. *J Physiol* 577:815–828.
22. Campenot RB (1994) NGF and the local control of nerve terminal growth. *J Neurobiol* 25:599–611.
23. Lawson JJ, McIlwrath SL, Woodbury CJ, Davis BM, Koerber HR (2008) TRPV1 unlike TRPV2 is restricted to a subset of mechanically insensitive cutaneous nociceptors responding to heat. *J Pain* 9:298–308.
24. Sleeper AA, et al. (2000) Changes in expression of two tetrodotoxin-resistant sodium channels and their currents in dorsal root ganglion neurons after sciatic nerve injury but not rhizotomy. *J Neurosci* 20:7279–7289.
25. Maricich SM, et al. (2009) Merkel cells are essential for light-touch responses. *Science* 324:1580–1582.
26. Loewenstein WR, Mendelson M (1965) Components of receptor adaptation in a Pacinian corpuscle. *J Physiol* 177:377–397.
27. Drew LJ, et al. (2004) Acid-sensing ion channels ASIC2 and ASIC3 do not contribute to mechanically activated currents in mammalian sensory neurones. *J Physiol* 556:691–710.
28. Elg S, Marmigere F, Mattsson JP, Ernfors P (2007) Cellular subtype distribution and developmental regulation of TRPC channel members in the mouse dorsal root ganglion. *J Comp Neurol* 503:35–46.
29. Honoré E, Maingret F, Lazdunski M, Patel AJ (2002) An intracellular proton sensor commands lipid- and mechano-gating of the K(+) channel TREK-1. *EMBO J* 21: 2968–2976.
30. Wetzel C, et al. (2007) A stomatin-domain protein essential for touch sensation in the mouse. *Nature* 445:206–209.
31. Maroto R, et al. (2005) TRPC1 forms the stretch-activated cation channel in vertebrate cells. *Nat Cell Biol* 7:179–185.
32. Staaf S, et al. (2009) Down regulation of TRPC1 by shRNA reduces mechanosensitivity in mouse dorsal root ganglion neurons in vitro. *Neurosci Lett* 457:3–7.
33. Halata Z, Grim M, Bauman KI (2003) Friedrich Sigmund Merkel and his "Merkel cell," morphology, development, and physiology: Review and new results. *Anat Rec A Discov Mol Cell Evol Biol* 271:225–239.
34. Hjerling-Leffler J, Alqatari M, Ernfors P, Koltzenburg M (2007) Emergence of functional sensory subtypes as defined by transient receptor potential channel expression. *J Neurosci* 27:2435–2443.
35. Desfrere L, et al. (2009) Na,K-ATPase signal transduction triggers CREB activation and dendritic growth. *Proc Natl Acad Sci USA* 106:2212–2217.

NEUROSCIENCE
Downloaded at Palestinian Territory, occupied on December 17, 2021
www.manaraa.com